Some properties of the Schwarzschild–de Sitter and Schwarzschild–anti-de Sitter spacetimes

Z. Stuchlík* and S. Hledík†
Department of Physics, Faculty of Philosophy and Science, Silesian University, Bezručovo nám. 13, 746 01 Opava, Czech Republic
(Received 12 March 1999; published 8 July 1999)

Properties of the Schwarzschild–de Sitter and Schwarzschild–anti-de Sitter spacetimes are characterized by three phenomena, namely, by the ''effective potential'' of the motion of test particles and photons, the photon escape cones, and the embedding diagrams of $t=$const sections of central planes of both the ordinary and optical reference geometry of these spacetimes. The phenomena are related to the corresponding phenomena of the Schwarzschild spacetime, and differences caused by the asymptotic structure of the spacetimes with a nonzero cosmological constant are discussed. The properties of the embedding diagrams of the optical geometry are related to the dynamical behavior of test particles. The limits of the embeddability of the optical geometry are given and compared with the limits on the outer radius of the interior solutions of Einstein's equations with a nonzero cosmological constant for static, spherically symmetric configurations of uniform density. It is shown that, contrary to the pure Schwarzschild case, these limits do not fully coincide for repulsive cosmological constants. [S0556-2821(99)05714-8]

PACS number(s): 04.70.Bw, 04.25.−g

I. INTRODUCTION

All recently available data from cosmological observations, including measurements of the present value of the Hubble parameter and dynamical estimates of the present energy density of the Universe, measurements of the anisotropy of the microwave cosmic relic radiation, statistics of the gravitational lensing of quasars and active galactic nuclei, galaxy number counts, and the measurements of high-redshift supernovae, give strong suggestions that in the framework of inflationary cosmology a nonzero repulsive cosmological constant, $\Lambda>0$, has to be invoked in order to explain the properties of the presently observed Universe [1–3]. The presence of a repulsive cosmological constant alters in a significant way asymptotic character of black-hole spacetimes. We shall discuss modifications of the character of the simplest, spherically symmetric spacetimes described by the Schwarzschild–de Sitter solutions of Einstein's equations. (However, we shall not consider Schwarzschild–de Sitter spacetimes with supercritical values of Λ which are dynamic everywhere.)

On the other hand, it has been shown recently that the anti-de Sitter spacetimes play an important role in the superstring theory [4]. Therefore, it is useful to investigate also the influence of an attractive cosmological constant $\Lambda<0$ on the black-hole solutions. We restrict our attention again to the simplest case of the spherically symmetric, Schwarzschild–anti-de Sitter spacetimes.

We shall estimate at which regions properties of both the Schwarzschild–de Sitter and Schwarzschild–anti-de Sitter spacetimes become significantly different than the corresponding properties of the pure Schwarzschild spacetime (with $\Lambda=0$). The modifications will be tested by using three phenomena that can be both astrophysically relevant and illustrative.

In Sec. II, an appropriate ''effective potential'' governing the radial motion of test particles and a ''generalized effective potential'' for the radial motion of photons are given. The effect of a nonzero cosmological constant is clearly reflected by their asymptotic behavior.

In Sec. III, impact of the asymptotic behavior of the spacetimes with a nonzero cosmological constant on the character of the photon escape cones related to the family of static observers is illustrated.

In Sec. IV, embedding diagrams of $t=$const sections of central planes of both the ordinary geometry and optical reference geometry associated with the Schwarzschild–de Sitter and Schwarzschild–anti-de Sitter spacetimes are constructed, and compared with the corresponding embedding diagrams of the Schwarzschild spacetime. The embedding diagrams give in an illustrative way information on changes of the spacetime structure caused by the presence of a nonzero cosmological constant. The embeddings of the optical reference geometry into the three-dimensional Euclidean space cannot be constructed for the whole static part of the spacetimes; the limits of embeddability are established. In the case of the Schwarzschild–anti-de Sitter spacetimes even the embeddability of the ordinary geometry is limited.

In Sec. V, relations between the limits of embeddability of the optical reference geometry of the vacuum spherically symmetric spacetimes with $\Lambda\neq0$ and the limits on the outer radius of interior solutions of Einstein's equations with $\Lambda\neq0$ for static and spherically symmetric configurations of uniform density are discussed. Further, it is shown that the limit of embeddability of the ordinary geometry is related to a special class of the interior solutions of Einstein's equations with $\Lambda<0$.

In Sec. VI, concluding remarks concerning differences of the properties of the Schwarzschild–de Sitter and Schwarzschild–anti-de Sitter spacetimes and the pure Schwarzschild spacetime are presented.

II. THE MOTION OF TEST PARTICLES AND PHOTONS

In the standard Schwarzschild coordinates (t,r,θ,ϕ), and the geometric system of units $(c=G=1)$, the

*Email address: Zdenek.Stuchlik@fpf.slu.cz
†Email address: Stanislav.Hledik@fpf.slu.cz

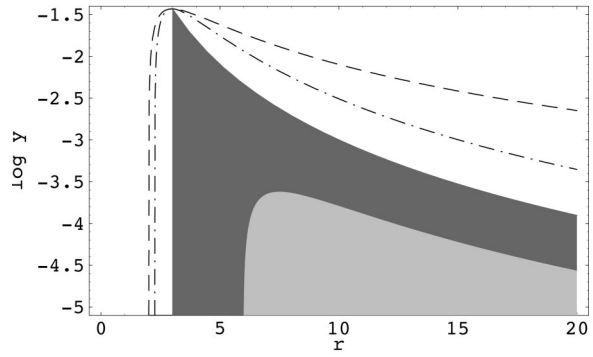

FIG. 1. Characteristic functions of the Schwarzschild–de Sitter spacetimes: $y_h(r)$ (dashed line) determines loci of the black-hole (the inner one) and cosmological (the outer one) horizons; $y_{e(\mathrm{opt})}(r)$ (dashed-dotted line) determines limits of embeddability of the central planes of the optical reference geometry into three-dimensional Euclidean space; $r=3$ and $y_s(r)$ determine limits of unstable circular orbits (dark shaded region); $y_{\mathrm{ms}}(r)$ determines limits of stable circular orbits (light shaded region). Notice that limits on existence of the static configurations of uniform density are determined by $y_{e(\mathrm{opt})}(r)$ at $r<3$, but by $y_s(r)$ at $r>3$.

Schwarzschild–de Sitter ($\Lambda>0$), and Schwarzschild–anti-de Sitter ($\Lambda<0$) spacetimes are determined by the line element

$$ds^2=-\left(1-\frac{2M}{r}-\frac{\Lambda}{3}r^2\right)dt^2+\left(1-\frac{2M}{r}-\frac{\Lambda}{3}r^2\right)^{-1}dr^2+r^2(d\theta^2+\sin^2\theta\, d\phi^2), \tag{1}$$

where M is the mass parameter of these spacetimes. However, it is useful to introduce a dimensionless parameter

$$y=\Lambda M^2/3, \tag{2}$$

and use dimensionless coordinates $t\to t/M$, $r\to r/M$. It is equivalent to putting $M=1$. The event horizons of the geometry (1) are then given by the condition

$$g_{tt}\equiv 1-\frac{2}{r}-yr^2=0. \tag{3}$$

The loci of the event horizons are determined by the relation

$$y=y_h(r)\equiv\frac{r-2}{r^3}; \tag{4}$$

the function $y_h(r)$ is illustrated in Figs. 1 and 4. In the Schwarzschild–de Sitter spacetimes, two event horizons exist if $0<y<y_{\mathrm{crit}}=1/27$. The black-hole horizon is located at

$$r_h=\frac{1}{\sqrt{3y}}\cos\frac{\pi+\xi}{3}, \tag{5}$$

the cosmological horizon at

$$r_c=\frac{1}{\sqrt{3y}}\cos\frac{\pi-\xi}{3}, \tag{6}$$

where

$$\xi=\cos^{-1}(3\sqrt{3}y). \tag{7}$$

The spacetime is dynamic at $r<r_h$ and $r>r_c$. If $y=y_{\mathrm{crit}}=1/27$, the horizons coincide at $r_h=3$. If $y>1/27$, the spacetime is dynamic at all $r>0$. In the Schwarzschild–anti-de Sitter spacetimes, a black-hole horizon always exist, and its location is determined by the relation

$$r_h=\left(-\frac{1}{y}\right)^{1/2}\left\{\left[1+\left(1-\frac{1}{27y}\right)^{1/2}\right]^{1/3}+\left[1-\left(1-\frac{1}{27y}\right)^{1/2}\right]^{1/3}\right\}. \tag{8}$$

The motion of test particles and photons is governed by the geodesic structure of the spacetime. The geodesic equation reads

$$\frac{Dp^\mu}{d\lambda}=0, \tag{9}$$

where $p^\mu\equiv dx^\mu/d\lambda$ is the four-momentum, and λ is the affine parameter. The normalization condition reads

$$p^\mu p_\mu=-m^2, \tag{10}$$

where m is the rest mass of test particles; $m=0$ for photons.

It follows from central symmetry of the geometry (1) that the motion of test particles and photons is allowed in the central planes only. Because of the existence of the time Killing vector $\boldsymbol{\xi}_{(t)}=\partial/\partial t$ and the axial one $\boldsymbol{\xi}_{(\phi)}=\partial/\partial\phi$, two constants of motion, which are the projections of the four-momentum onto the Killing vectors, must exist:

$$p_t=g_{t\mu}p^\mu=-\mathcal{E},\quad p_\phi=g_{\phi\mu}p^\mu=\Phi. \tag{11}$$

In the spacetimes with a nonzero cosmological constant, the constants of motion $\mathcal{E}$ and Φ cannot be interpreted as energy and axial component of the angular momentum at infinity, since their geometry is not asymptotically flat. It should be, therefore, interesting to discuss a possibility to find regions of these spacetimes which have character that is ''close'' to the character of the Schwarzschild spacetime.

It is useful to introduce specific energy E, specific angular momentum L and impact parameter l by the relations

$$E=\frac{\mathcal{E}}{m},\quad L=\frac{\Phi}{m},\quad l=\frac{\Phi}{\mathcal{E}}. \tag{12}$$

If we choose the plane of the motion to be the equatorial plane ($\theta=\pi/2$), we find that the motion of test particles ($m\neq 0$) is determined by an ''effective potential'' [5]

$$V_{\mathrm{eff}}(r;L,y)\equiv\left(1-\frac{2}{r}-yr^2\right)\left(1+\frac{L^2}{r^2}\right). \tag{13}$$

The motion is allowed in regions where

$$E^2 \geqslant V_{\rm eff}(r;L,y), \tag{14}$$

and the turning points of the radial motion are determined by the condition $E^2 = V_{\rm eff}(r;L,y)$.

The radial motion of photons ($m=0$) can be determined by a ''generalized effective potential,'' related to the impact parameter l. The motion is allowed in regions where

$$l^2 \leqslant l_R^2(r;y) \equiv \frac{r^3}{r-2-yr^3}, \tag{15}$$

the condition $l^2 = l_R^2(r;y)$ gives the turning points of the radial motion.

The functions $V_{\rm eff}(r;L,y)$ and $l_R^2(r;y)$ are defined between the black-hole and cosmological horizons in the case of the Schwarzschild–de Sitter spacetimes; $V_{\rm eff}$ is zero at the horizons, while l_R^2 diverges there. The functions are defined at all radii above the black-hole horizons in the case of the Schwarzschild–anti-de Sitter spacetimes; $V_{\rm eff}$ is zero at the horizon, while l_R^2 diverges there. Purely radial motion (with $L=0$, or $l=0$) was discussed in Ref. [6].

Circular orbits of test particles correspond to local extrema ($\partial V_{\rm eff}/\partial r = 0$) of the effective potential. Maxima ($\partial^2 V_{\rm eff}/\partial r^2 < 0$) determine unstable circular orbits, minima ($\partial^2 V_{\rm eff}/\partial r^2 > 0$) determine stable circular orbits. The specific energy and specific angular momentum of particles on circular orbits are determined by the relations [5]

$$E_c(r;y) = \left(1 - \frac{2}{r} - yr^2\right)\left(1 - \frac{3}{r}\right)^{-1/2}, \tag{16}$$

$$L_c(r;y) = [r(1-yr^3)]^{1/2}\left(1 - \frac{3}{r}\right)^{-1/2}. \tag{17}$$

The circular orbits can exist at radii limited by

$$3 < r \leqslant r_s \equiv y^{-1/3}. \tag{18}$$

At $r=3$, both E_c and L_c diverge; a photon circular orbit exists there. It is given by a local minimum of the function $l_R^2(r;y)$, which is located at $r=3$ independently of the value of the cosmological parameter y. Of course, the impact parameter of the photon circular orbit depends on y:

$$l_c^2(y) = \frac{27}{1-27y}. \tag{19}$$

Thus, similarly to the ''pure'' Schwarzschild case, the radii of circular orbits are limited from below by the photon circular orbit at $r=3$. In the case of the Schwarzschild–anti-de Sitter spacetimes ($y<0$), this is the only restriction. Further, we shall discuss the properties of the effective potentials separately in the cases $y>0$ and $y<0$.

A. The Schwarzschild–de Sitter spacetimes

The radii of circular orbits are limited from above at so called static radius, where the gravitational attraction invoked by the mass of the source is just compensated by the cosmological repulsion. The static radius is given by the condition

$$y = y_s(r) \equiv \frac{1}{r^3}; \tag{20}$$

$y_s(r)$ is illustrated in Fig. 1. At the static radius, particles with the specific energy

$$E_s(y) = (1-3y^{1/3})^{1/2}, \tag{21}$$

(and $L=0$) are at an unstable equilibrium.

The stable circular orbits exist at radii limited by the relation

$$4yr^4 - 15yr^3 - r + 6 \leqslant 0. \tag{22}$$

The marginally stable orbits are given by

$$y = y_{\rm ms}(r) \equiv \frac{r-6}{r^3(4r-15)}. \tag{23}$$

The function $y_{\rm ms}(r)$ is illustrated in Fig. 1. Its zero is at $r=6$, corresponding to the marginally stable circular orbit in the Schwarzschild spacetime. The function $y_{\rm ms}(r)$ diverges at $r=0$, and at $r=15/4$; $y_{\rm ms} \to +\infty$ for $r \to 0$, and if $r \to 15/4$ from below, and it has a minimum at $r=3$, where $y_{\rm ms}=1/27$. However, the function $y_{\rm ms}(r)$ is physically irrelevant at whole the range $0<r<15/4$, because $y_{\rm ms}(r) > 1/27$ there, i.e., it corresponds to spacetimes that are dynamical at all $r>0$. The physically relevant part of $y_{\rm ms}(r)$ is located at $r \geqslant 6$. Its maximum is located at $r_{c({\rm ms})}=15/2$, and the maximum value of the cosmological parameter allowing existence of stable circular orbits is

$$y_{c({\rm ms})} = \frac{12}{15^4} \simeq 0.000237. \tag{24}$$

The corresponding critical value of Schwarzschild mass $M_{c({\rm ms})} = (3y_{c({\rm ms})}/\Lambda)^{1/2}$; considering an upper limit on the cosmological parameter $\Lambda \sim 10^{-55}\,{\rm cm}^{-2}$ [7], we find

$$M_{c({\rm ms})} \approx 8.43 \times 10^{25}\ {\rm cm} \sim 5.75 \times 10^{20} M_\odot. \tag{25}$$

The behavior of the effective potential is illustrated for three typical situations ($y > y_{c({\rm ms})}$, $y < y_{c({\rm ms})}$, $y \ll y_{c({\rm ms})}$) in Fig. 2.

B. The Schwarzschild–anti-de Sitter spacetimes

In this case, the asymptotical behavior of the functions determining motion of test particles and photons has radically different character, and it is given by

$$V_{\rm eff}(r \to \infty; y) \sim -yr^2, \quad l_R^2(r \to \infty, y) \sim -y^{-1}. \tag{26}$$

The effective potential is illustrated again for three typical situations (with the same magnitude of y as in the Schwarzschild–de Sitter case) in Fig. 3. Now, the stable circular orbits can exist for all values of the attractive cosmological parameter. The marginally stable orbits are again de-

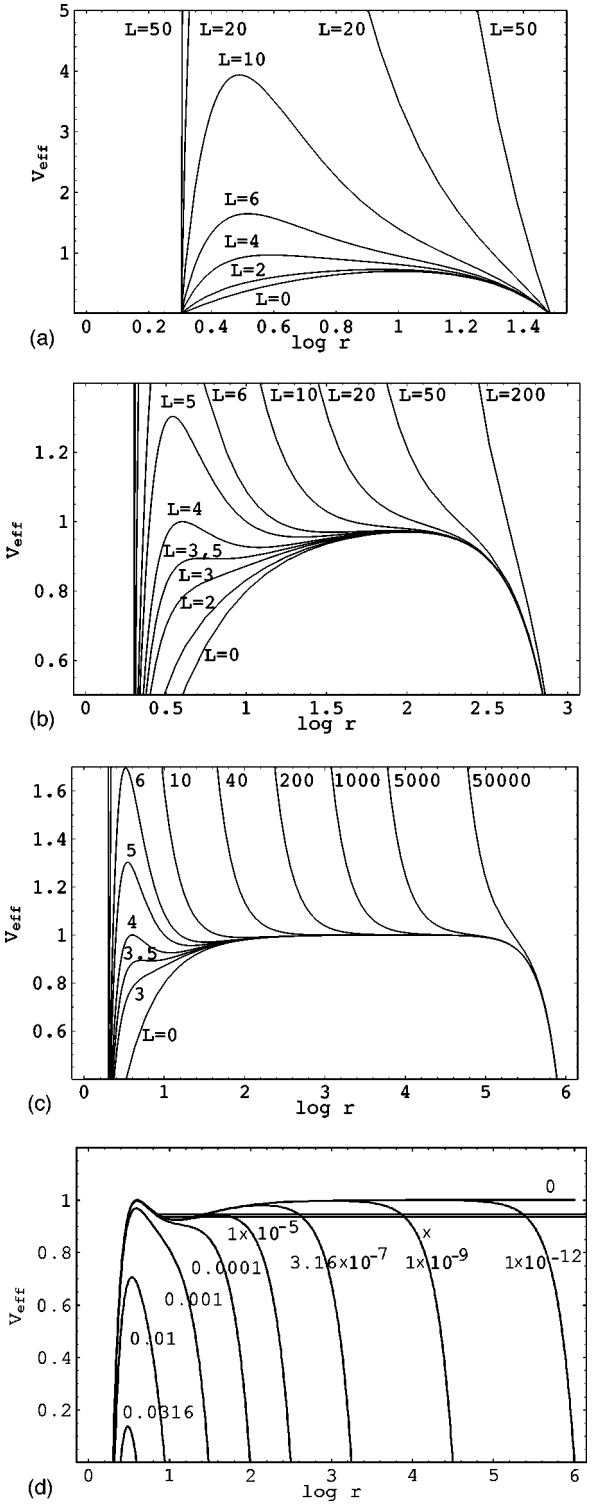

FIG. 2. Effective potential of the test-particle motion in the Schwarzschild–de Sitter spacetimes. The potential is given for various specific axial momenta for the spacetimes with (a) $y=10^{-3}>y_{c(\mathrm{ms})}\approx 0.000237$, when stable circular orbits cannot exist, (b) $y=10^{-6}$ and (c) $y=10^{-12}$, when stable circular orbit, corresponding to minima of the effective potential, are possible. For comparison, in (d), the effective potential is given for various values of y, with $L=4$ fixed.

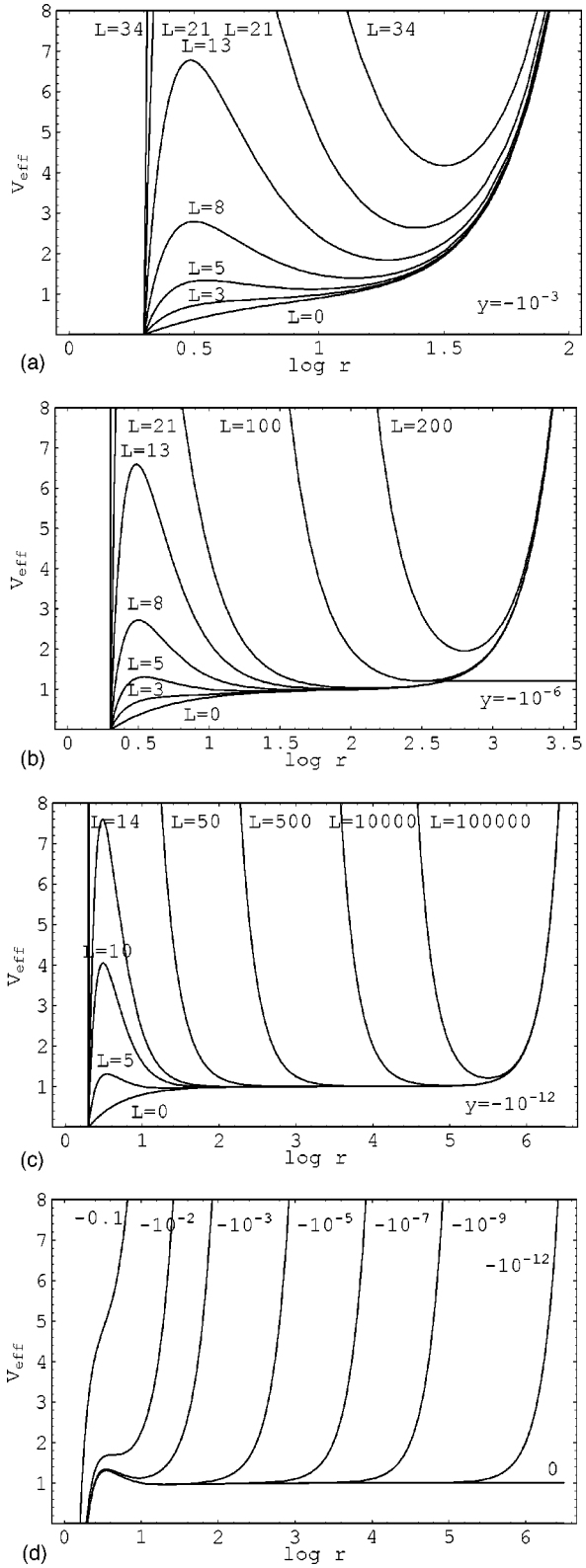

FIG. 3. Effective potential of the test-particle motion in the Schwarzschild–anti-de Sitter spacetimes. The potential is given for various specific angular momenta for the spacetimes with (a) $y=-10^{-3}$, (b) $y=-10^{-6}$, (c) $y=-10^{-12}$. For all $y<0$ the effective potential has the same character; stable circular orbits are possible in all the cases with $y<0$. For comparison, in (d), the potential is given for various $y<0$ with $L=5$ fixed.

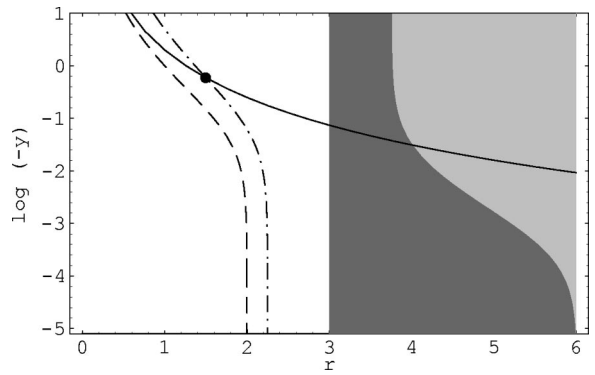

FIG. 4. Characteristic functions of the Schwarzschild–anti-de Sitter spacetimes: $y_h(r)$ (dashed line) determines loci the black-hole event horizon; $y_{e(\mathrm{opt})}(r)$ (dashed-dotted line) determines limits of embeddability of the optical geometry onto Euclidean space; $r=3$ gives limit on existence of unstable circular orbits (dark shaded region); $y_{\mathrm{ms}}(r)$ determines limit of stable circular orbits (light shaded region); $y_{e(\mathrm{ord})}(r)$ (solid line) determines limit of embeddability of the ordinary geometry (of the central planes of $t=$const sections) into the Euclidean geometry. Limits on existence of the static configurations of uniform density are given by the function $y_{e(\mathrm{opt})}$. Above the intersection of $y_{e(\mathrm{ord})}(r)$ and $y_{e(\mathrm{opt})}(r)$ (at the point $r=3/2$, $y=-16/27$) the static configurations of uniform density, characterized by the function $y_{e(\mathrm{ord})}(r)$, cannot exist.

termined by the relation (23); their radii shift from $r_{\mathrm{ms}}\to 6$ (for $y\to 0$) to $r_{\mathrm{ms}}\to 15/4$ (for $y\to-\infty$).

For the Schwarzschild–anti-de Sitter spacetimes, the loci of the black-hole horizon, the circular photon orbit, and the marginally stable circular orbit are illustrated in Fig. 4. The ''generalized effective potential'' for the photon motion $l_R^2(r;y)$ is illustrated in Fig. 5, for the spacetimes with both $y>0$ and $y<0$.

III. PHOTON ESCAPE CONES

We shall demonstrate the influence of both repulsive and attractive cosmological constant on the behavior of photon escape cones related to the family of static observers. Although measured by local observers, the photon escape cones

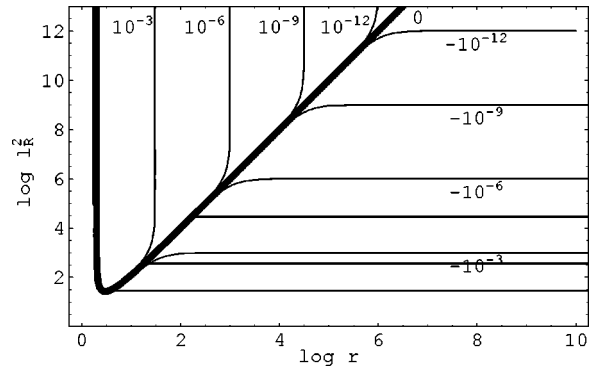

FIG. 5. The generalized ''effective potential'' of the photon motion in both the Schwarzschild–de Sitter and Schwarzschild–anti-de Sitter spacetimes. The generalized effective potential is related to the impact parameter.

reflect global properties of the spacetimes under consideration.

The tetrad of vectors carried by the static observers is

$$\boldsymbol{e}_{(t)}=\left(1-\frac{2}{r}-yr^2\right)^{1/2}\frac{\partial}{\partial t}, \tag{27}$$

$$\boldsymbol{e}_{(r)}=\left(1-\frac{2}{r}-yr^2\right)^{-1/2}\frac{\partial}{\partial r}, \tag{28}$$

$$\boldsymbol{e}_{(\theta)}=\frac{1}{r}\frac{\partial}{\partial\theta}, \tag{29}$$

$$\boldsymbol{e}_{(\phi)}=\frac{1}{r\sin\theta}\frac{\partial}{\partial\phi}. \tag{30}$$

The components of the four-momentum of a photon as measured by a static observer are

$$p_{(\alpha)}=p_\mu \boldsymbol{e}^\mu_{(\alpha)}. \tag{31}$$

Using relations $p^{(t)}=-p_{(t)}$, $p^{(\phi)}=p_{(\phi)}$, $p^{(r)}=p_{(r)}$, we can find the directional angle ψ of the photon (i.e., the angle measured by the observer relative to its outward radial direction) to be given by the relations

$$\sin\psi=\frac{p^{(\phi)}}{p^{(t)}}=\left(1-\frac{2}{r}-yr^2\right)^{1/2}\frac{l}{r}, \tag{32}$$

$$\cos\psi=\frac{p^{(r)}}{p^{(t)}}=\pm\left[1-\left(1-\frac{2}{r}-yr^2\right)\frac{l^2}{r^2}\right]^{1/2}. \tag{33}$$

The photon escape cones can be determined by using the function $l_R^2(r;y)$ governing the photon motion. In establishing the directional angle ψ_c of an marginally escaping photon, the impact parameter l_c of the unstable circular photon orbit plays the crucial role for static observers located both under and above the circular photon orbit at $r=3$; for simplicity we consider only positive values of l_c because the cone is symmetric about the radial direction. At $r=3$, the escape angle is

$$\psi_c(r=3;y)=\frac{\pi}{2}, \tag{34}$$

independently of y. Directional escaping angles at $r\neq 3$ can be determined by inserting the formula for l_c into Eqs. (32) and (33). We arrive at the expressions

$$\sin\psi_c(r;y)=\left(\frac{27(r-2-yr^3)}{r^3(1-27y)}\right)^{1/2}, \tag{35}$$

$$\cos\psi_c(r;y)=\pm\left(\frac{r^3-27r+54}{r^3(1-27y)}\right)^{1/2}, \tag{36}$$

which reduce to the ''Schwarzschild'' ($y=0$) formulas

$$\sin\psi_c(r)=\left(\frac{27(r-2)}{r^3}\right)^{1/2}, \tag{37}$$

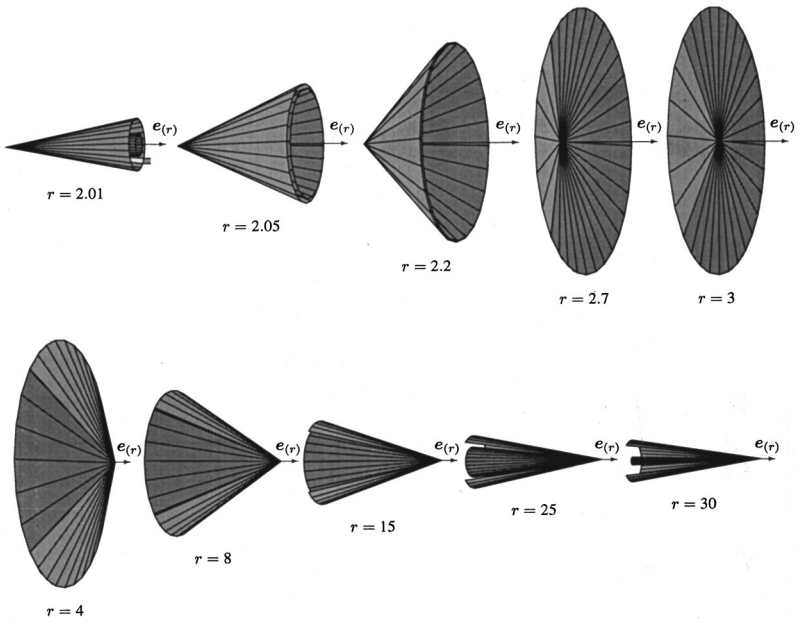

FIG. 6. Photon escape cones in the Schwarzschild–de Sitter spacetimes. The cones given at typical radii in the spacetime with $y = 10^{-3}$ are compared with the corresponding cones in the pure Schwarzschild spacetime ($y = 0$). Close to the black-hole horizon (e.g., at $r = 2.01$), the escape cone of the Schwarzschild–de Sitter spacetime (dark gray) is significantly narrower than the Schwarzschild one (light gray). As r tends to $r = 3$, corresponding to the radius of photon circular orbits, the cones become closer, and they coincide at $r = 3$, where the opening angle $\psi = \pi/2$. At $r > 3$, the Schwarzschild escape cone becomes narrower than the Schwarzschild–de Sitter cone (with $\psi > \pi/2$). The complementary photon capture cone is narrower in the Schwarzschild–de Sitter spacetime; the differences can be significant close to the cosmological horizon.

$$\cos\psi_c(r) = \pm\left(1 - \frac{27}{r^2} + \frac{54}{r^3}\right)^{1/2}. \tag{38}$$

For $r < 3$, the marginally escaping photon is radially outward directed ($p^{(r)} > 0$ and $\cos\psi_c$ is taken with the plus sign), for $r > 3$, it is inwards directed ($p^{(r)} < 0$ and $\cos\psi_c$ is taken with the minus sign).

A. The Schwarzschild–de Sitter spacetimes

The behavior of the escape cones is presented in Fig. 6. At a fixed (and allowed) $r < 3$, the escape cone of the Schwarzschild spacetime is the widest one, and it gets smaller with y growing. On the other hand, at a fixed (and allowed) $r > 3$, the Schwarzschild escape cone is the smallest one. Of course, the complementary Schwarzschild photon capture cone is the widest one at $r > 3$. Close to the cosmological horizon, the Schwarzschild–de Sitter capture cone gets to be strongly narrower than the Schwarzschild capture cone, as one can expect intuitively.

B. The Schwarzschild–anti-de Sitter spacetimes

The behavior of the escape cones is presented in Fig. 7. At a fixed (and allowed) $r < 3$, the escape cone of the Schwarzschild spacetime is the narrowest one; it gets wider with y descending. At a fixed $r > 3$, the Schwarzschild escape cone becomes greater than the cones with $y < 0$. The complementary photon capture cone of the pure Schwarzschild spacetime lies inside the capture cones of the spacetimes with $y < 0$. Asymptotically (for $r \to \infty$), the Schwarzschild capture cone degenerates into the inward radial direction, while the Schwarzschild–anti-de Sitter cone converges to an opening angle which is nonzero. One can find that

$$\sin\psi_c(r \to \infty; y < 0) \sim 3\left(\frac{3y}{27y - 1}\right)^{1/2}. \tag{39}$$

This behavior of the escape cones clearly illustrates modified asymptotic character of the Schwarzschild–anti-de Sitter spacetimes.

IV. EMBEDDING DIAGRAMS

Curvature of static parts of the vacuum, spherically symmetric black-hole spacetimes with a nonzero cosmological constant can be conveniently illustrated by embedding diagrams. Comparison of these embedding diagrams with those constructed for the pure Schwarzschild spacetimes [8,9] gives an intuitive insight into the change of the character of the spacetime caused by the cosmological constant. It is useful for both ordinary and optical geometry.

The existence of the field of the time Killing vector $\partial/\partial t$ enables us to define a privileged notion of space using the hypersurfaces of $t = \text{const}$. First, we shall use the induced metric on these hypersurfaces (i.e., the space components of the metric tensor g_{ik})—we call it ordinary space. Then, we shall consider so called optical reference geometry referred to the $t = \text{const}$ hypersurfaces by an appropriate conformal

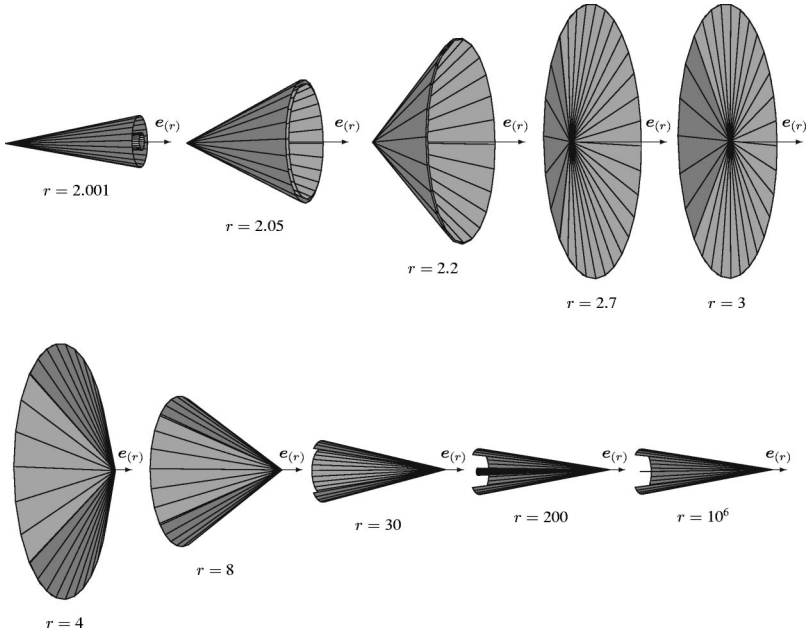

FIG. 7. Photon escape cones in the Schwarzschild–anti-de Sitter spacetimes. The cones are given at typical radii for the spacetime with $y=-10^{-3}$ (dark gray), and compared with the corresponding Schwarzschild cones (light gray). Contrary to the situation in the spacetimes with $y>0$, in the Schwarzschild–anti-de Sitter spacetimes the escape cone is wider than the Schwarzschild escape cone at $r<3$. They coincide at $r=3$, again. At $r>3$, the Schwarzschild capture cone is narrower than the Schwarzschild–anti-de Sitter capture cone. As r tends to infinity, the difference between both cones becomes more evident, while the Schwarzschild capture cone degenerates into a radial inward directed line, the Schwarzschild–anti-de Sitter capture cone converges to a constant-angle cone.

scaling [9]. Geometry of all the central planes of these hypersurfaces is the same as those of the equatorial plane ($\theta=\pi/2$) as a consequence of the central symmetry of the spherically symmetric spacetimes. Therefore, the embedding diagrams will be constructed for the equatorial plane in all the considered cases.

A. Embedding of the ordinary geometry

We shall embed the surface described by the line element

$$dl^2_{(\mathrm{S-deS})}=\left(1-\frac{2}{r}-yr^2\right)^{-1}dr^2+r^2d\phi^2, \tag{40}$$

corresponding to the equatorial plane of $t=$const hypersurface, into a flat Euclidean three-dimensional space whose line element is in the standard cylindrical coordinates given by

$$d\sigma^2=d\rho^2+\rho^2d\phi^2+dz^2. \tag{41}$$

The embedding is given by the surface $z=z(\rho)$, which have to isometric with the equatorial plane of the $t=$const hypersurface of the spacetime. Thus we have to identify the line element given by

$$dl^2_{(E)}=\left[1+\left(\frac{dz}{d\rho}\right)^2\right]d\rho^2+\rho^2d\phi^2 \tag{42}$$

with the line element (40).

We can identify the azimuthal coordinates ϕ; moreover, in the case of the ordinary space, also the radial coordinates r and ρ can be identified. The embedding diagram can then be given by the formula $z=z(r)$, which can be obtained by integrating the relation

$$\frac{dz}{dr}=\pm\left(\frac{2+yr^3}{r-2-yr^3}\right)^{1/2}. \tag{43}$$

The choice of the positive or negative sign in Eq. (43) leads to isometric surfaces, and is therefore irrelevant.

1. The Schwarzschild–de Sitter spacetimes

In the case of a repulsive cosmological constant, the embedding can be constructed for complete static regions between the black-hole (r_h) and cosmological (r_c) horizons. Recall that the static region exists for $y\leqslant 1/27$ only. The embeddings are given for several typical values of y ($0<y<1/27$) in Fig. 8; the pure Schwarzschild case ($y=0$) is included for comparison. The presence of a repulsive cosmological constant alters the character of the embedding diagram substantially in comparison with the case of $y=0$. Due to the asymptotical behavior of the Schwarzschild–de Sitter spacetimes, the embedding diagrams have a shape corresponding to a funnel—a throat corresponds to both the black-hole and cosmological horizons. With y growing, distance between the horizons decreases, and the height of the diagram decreases too. The shape of the embedding diagram becomes closer and closer to a cylindrical surface with more and more limited height. With $y\to 1/27$ the diagram is shrinking to the circle of radius $r=3$.

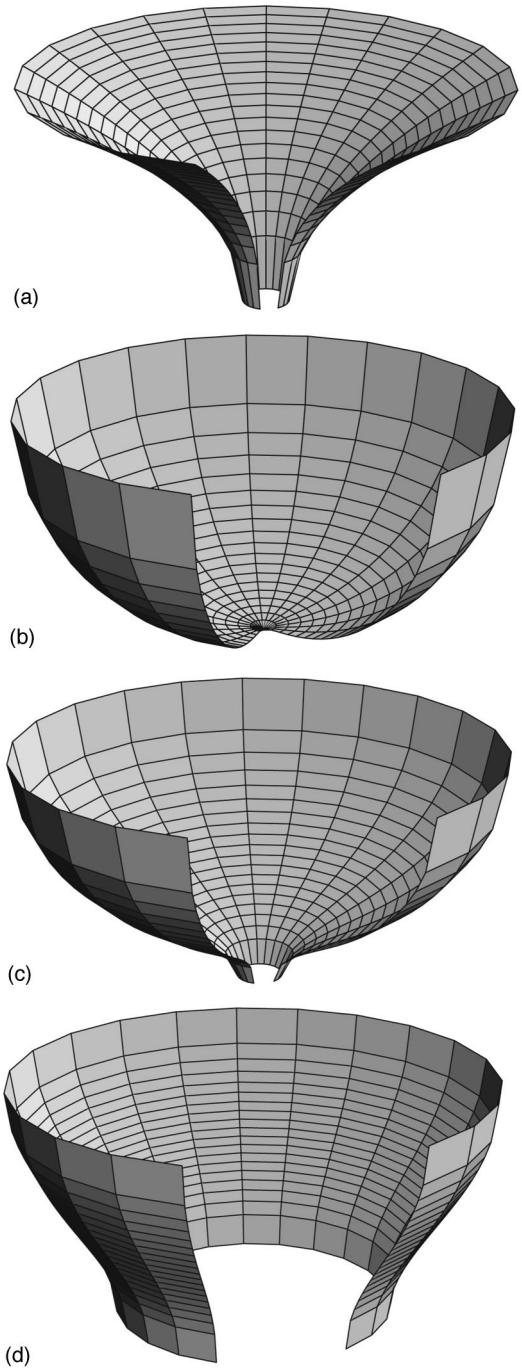

FIG. 8. Embedding diagrams of the ordinary induced geometry of $t=$ const sections of the Schwarzschild–de Sitter spacetimes. The pure Schwarzschild case ($y=0$) is taken for comparison in (a). The diagrams are given for (b) $y=10^{-6}$, (c) $y=0.002$, and (d) $y=0.03$. For $y=0$ the diagram is asymptotically flat [see (a)]. For $0<y<1/27$, the diagram resembles a funnel having a throat at both the black-hole and cosmological horizons. Note that both r and z scales are adjusted so that all the plots occupy approximately the same area. For real proportions, see Fig. 10.

2. The Schwarzschild–anti-de Sitter spacetimes

In the case of an attractive cosmological constant, the static region extends from the black-hole horizon to infinity.

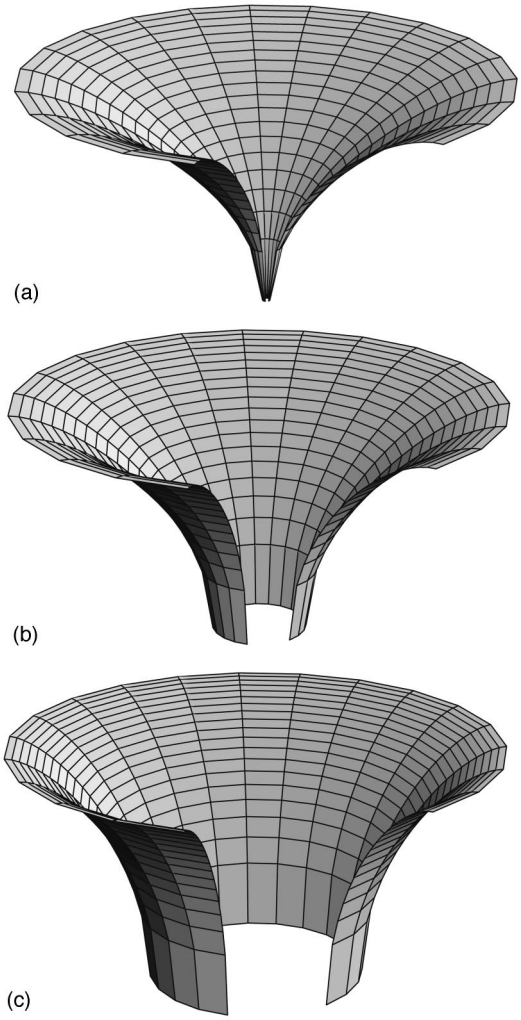

FIG. 9. Embedding diagrams of the ordinary geometry of $t=$ const section of the Schwarzschild–anti-de Sitter spacetimes. The diagrams are given for (a) $y=-10^{-6}$, (b) $y=-0.002$, (c) $y=-0.03$. Now, the embeddability into the Euclidean space is limited by the function $y_e(r)$. Note that both r and z scales are adjusted so that all the plots occupy approximately the same area. For real proportions, see Fig. 10.

However, we can see directly from Eq. (43) that the embedding diagrams of the ordinary space can be constructed in a limited part of the static region, located between the black-hole horizon r_h and $r_{e(\mathrm{ord})}=(-2/y)^{1/3}$. We shall characterize the limit of embeddability of the ordinary space by the condition

$$y \geqslant y_{e(\mathrm{ord})}(r) \equiv -\frac{2}{r^3}, \tag{44}$$

the function $y_{e(\mathrm{ord})}(r)$ is illustrated in Fig. 4.

The embedding diagrams of the ordinary induced geometry are given for several values of $y<0$ in Fig. 9. Now, in the region of embeddability, the embedding diagrams have a similar character as in the Schwarzschild case. But, contrary to the Schwarzschild [8] and Kerr [10] case, or the Schwarzschild–de Sitter case discussed above, where the

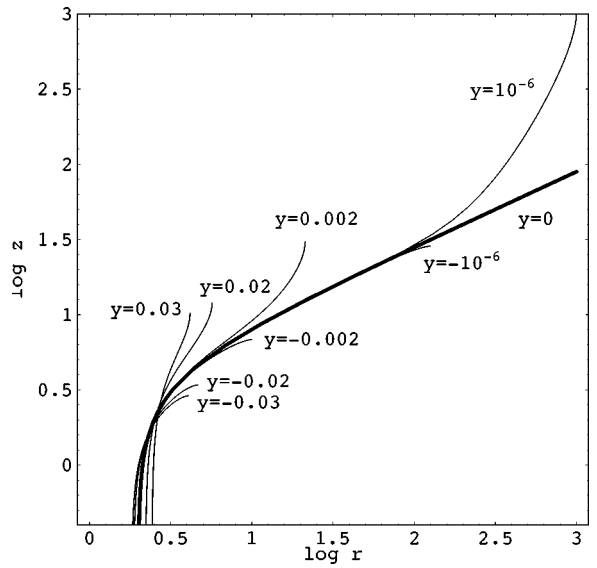

FIG. 10. Qualitative features of the embedding diagrams of the ordinary geometry of the Schwarzschild–de Sitter and Schwarzschild–anti-de Sitter spacetimes in a log-log diagram. One can immediately see how the diagrams with $y\neq 0$ ''peel off'' the pure Schwarzschild diagram ($y=0$, bold curve). All sections with $y\neq 0$ are complete (i.e., the maximum that can be embedded into Euclidean space is shown), except uninteresting lower parts of the throats. The diagrams clearly indicate modifications of the spacetime structure caused by the presence of a cosmological constant.

static part of the ordinary geometry can be embedded into the flat space completely, the embeddability of the ordinary geometry of the Schwarzschild–anti-de Sitter spacetime is limited by the condition (44). If the embeddability condition is satisfied, the rate of change of the circumferential length per unit increase of proper radial distance can be ''fit'' into the Euclidean space. In the opposite case, the space is still well defined, but the size of the circumferences grows faster than it does on a Euclidean plane, and no embedding in the Euclidean space is then possible [11]. Qualitative features of the modifications of the embedding diagrams of the ordinary geometry are illustrated by Fig. 10 (for both $y>0$ and $y<0$).

B. Embedding of the optical geometry

It is useful to consider the optical reference geometry defined on the hypersurfaces $t=\text{const}$ by conformal rescaling. The metric coefficients of the optical geometry are given by the relation [9]

$$\tilde{g}_{ik}=(g_{tt})^{-1}g_{ik}=\left(1-\frac{2}{r}-yr^2\right)^{-1}g_{ik}, \tag{45}$$

where g_{ik} are the metric coefficients of the ordinary geometry. The optical geometry differs significantly from the ordinary geometry and it reflects in a proper way some hidden properties of the spacetimes under consideration. The geodesics of the optical space are representing these properties. They coincide with trajectories of light, i.e., they are ''optically straight'' [12,13]; they are also ''dynamically straight,'' because test particles moving along geodesics of the optical geometry are kept on these trajectories by a force independent of their velocity [14]; they are also ''inertially straight,'' because a gyroscope carried along these geodesics does not precess along the direction of the motion [15]. It is well known that a vector representing the gyroscope's spin is parallelly transported on the surface $z=z(\rho)$ in the Euclidean space [15]. Therefore, the embedding diagrams of the optical geometry give a direct illustration of the precession of gyroscopes (see Ref. [11] for details).

For the equatorial section of the optical geometry related to the Schwarzschild–de Sitter and Schwarzschild–anti-de Sitter spacetimes, we have to identify the line element

$$d\tilde{l}_{(\mathrm{S-deS})}=\left(1-\frac{2}{r}-yr^2\right)^{-2}dr^2+r^2\left(1-\frac{2}{r}-yr^2\right)^{-1}d\phi^2 \tag{46}$$

with the line element (42), in order to construct the embedding diagram of the optical geometry. The azimuthal angles can again be directly identified. For the radial coordinates, however, we have to put

$$\rho=r\left(1-\frac{2}{r}-yr^2\right)^{-1/2}. \tag{47}$$

The embedding diagrams can be conveniently expressed using a parametric form of the embedding formula $z(\rho)=z[\rho(r)]$, with r being the parameter. Since

$$\frac{dz}{d\rho}=\frac{dz}{dr}\frac{dr}{d\rho}, \tag{48}$$

we arrive at the formula

$$\left(\frac{dz}{dr}\right)^2=\left(1-\frac{2}{r}-yr^2\right)^{-2}-\left(\frac{d\rho}{dr}\right)^2, \tag{49}$$

and finally

$$\frac{dz}{dr}=\pm\frac{r}{r-2-yr^3}\left[\frac{4r-9-yr^4}{r(r-2-yr^3)}\right]^{1/2}. \tag{50}$$

The embedding formula $z=z(\rho)$ can then be constructed by a numerical procedure. Further, it is immediately clear from Eq. (48) that ''turning radii'' of the embedding diagrams are given by the condition $d\rho/dr=0$. Since

$$\frac{d\rho}{dr}=\left(1-\frac{3}{r}\right)\left(1-\frac{2}{r}-yr^2\right)^{-3/2}, \tag{51}$$

we can see that the turning radius determining a throat of the embedding diagram of the optical geometry is located just at $r=3$, corresponding to the radius of the photon circular orbit; it is exactly the same result as that obtained in the pure Schwarzschild case. The radius of the photon circular orbit is important from the dynamical point of view, because the centrifugal force related to the optical geometry reverses its sign there [12,16]. Above the photon circular orbit, the dynamics is qualitatively Newtonian with the centrifugal force

directed towards increasing r. However, at $r=3$, the centrifugal force vanishes, and at $r<3M$ it is directed towards decreasing r. The photon circular orbit, the throat of the embedding diagram of the optical geometry ($d\rho/dr=0$), and vanishing centrifugal force, all appear at the radius $r=3$. It is simply given by the fact that the ''effective potential'' of the photon motion, the Euclidean coordinate ρ of the embedding, and the centrifugal force, all of them are determined by the azimuthal metric coefficient of the optical geometry

$$\tilde{g}_{\phi\phi}=r^2\left(1-\frac{2}{r}-yr^2\right)^{-1}. \tag{52}$$

It follows from Eq. (50) that embedding into the Euclidean space is possible, if the condition of embeddability

$$4r-9-yr^4\geqslant 0 \tag{53}$$

is satisfied. We shall express the limit of embeddability of the optical geometry by the relation

$$y=y_{e(\mathrm{opt})}(r)\equiv\frac{4r-9}{r^4}. \tag{54}$$

For $y=0$ we obtain the well known limit of embeddability of the optical geometry of the Schwarzschild spacetime $r_{e(\mathrm{opt})}=9/4$ (see Ref. [9]). The function $y_{e(\mathrm{opt})}(r)$ is illustrated in Fig. 1 for $y>0$, and in Fig. 4 for $y<0$.

1. The Schwarzschild–de Sitter spacetimes

The function $y_{e(\mathrm{opt})}(r)$ has its maximum at $r=3$, where $y_{e(\mathrm{opt})}=1/27=y_{\mathrm{crit}}$. Therefore, for all the Schwarzschild–de Sitter spacetimes containing a static region, the embeddability of the optical geometry is restricted both from below, and from above. Using a numerical procedure, the embedding diagrams are constructed for the same values of y as in the case of the ordinary geometry; they are given in Fig. 11. For $y\ll 1/27$, the embeddings of the optical geometry are very close to the embedding diagram of the optical geometry of the Schwarzschild spacetime. It is caused by the fact that the regions of the Schwarzschild–de Sitter spacetimes near the cosmological horizon, which have character significantly different from that corresponding to the Schwarzschild geometry, are ''cut off'' by the limit of embeddability given by Eq. (54). With y growing up to the critical value $y_{\mathrm{crit}}=1/27$, the embedding diagrams become restricted to a region symmetric around the turning radius at $r=3$. For $y=1/27$, the diagram degenerates into the circle at $r=3$, similarly to the case of the embedding diagrams of the ordinary geometry.

Of course, the optical space is still well defined outside the regions of the embeddability into the Euclidean space. It is useful to demonstrate its properties near the black-hole and cosmological horizons by the behavior of the proper lengths along the radial direction. In the optical geometry, the proper radial length coincides with the well known Regge-Wheeler ''tortoise'' coordinate:

$$r^*=\int\left(1-\frac{2}{r}-yr^2\right)^{-1}dr. \tag{55}$$

By integration (for $0<y<1/27$) we arrive at

$$r^*=A\ln\frac{|r-r_h|}{r+r_h+r_c}+B\ln\frac{|r_c-r|}{r+r_h+r_c}+A\left(\ln\frac{r_c}{r_h}-\frac{1}{2}\right), \tag{56}$$

where

$$A=\frac{r_h}{1-3yr_h^2},\quad B=\frac{r_c}{1-3yr_c^2}. \tag{57}$$

This gives direct meaning of the ''tortoise'' coordinate in the optical space. Clearly, the horizons are infinitely far away at the optical geometry; at $r\sim r_h$, $r^*\to-\infty$ ($r\sim r_c$, $r^*\to+\infty$) logarithmically. On the other hand, in the ordinary geometry, the horizons are located at a finite proper radial distance

$$\tilde{r}=\int\left(1-\frac{2}{r}-yr^2\right)^{-1/2}dr; \tag{58}$$

at $r\approx r_h$, $\tilde{r}\sim\sqrt{r-r_h}$, while at $r\approx r_c$, $\tilde{r}\approx\sqrt{r_c-r}$.

The optical space continues infinitely beyond the limit of embeddability, approaching asymptotically the geometry

$$d\tilde{\sigma}^2\approx dr^{*2}+\frac{r_h^3\exp(-r^*/A)}{y(r_c-r_h)(r_h-r_d)(2r_h+r_c)}\times(d\theta^2+\sin^2\theta\,d\phi^2) \tag{59}$$

for $r\to r_h$, $r^*\to-\infty$ and

$$d\tilde{\sigma}^2\approx dr^{*2}+\frac{r_c^3\exp(-r^*/B)}{y(r_c-r_h)(r_c-r_d)(2r_c+r_h)}\times(d\theta^2+\sin^2\theta\,d\phi^2) \tag{60}$$

for $r\to r_c$, $r^*\to+\infty$. Here

$$r_d=-\frac{1}{3y}\cos\frac{1}{3}\xi. \tag{61}$$

2. The Schwarzschild–anti-de Sitter spacetimes

Now the limiting condition (53) restricts embeddability of the optical geometry only from below (see Fig. 4); with $y\to-\infty$ the limit shifts to $r\to0$, along with the radius of the black-hole horizon. The embedding diagrams are constructed by the numerical procedure for the same values of y as for the ordinary space. They are given in Fig. 12. These diagrams have a special property, not present for the embedding diagrams in the other cases. Namely, they cover whole the asymptotic part of the Schwarzschild–anti-de Sitter spacetime, but in a restricted part of the Euclidean space. This is clear from the asymptotic behavior of $\rho(r)$. For $r\to+\infty$, there is $\rho\sim(-y)^{-1/2}$. Clearly, with decreasing attractive cosmological constant the embedding diagram is deformed with increasing intensity. The circles of $r=\mathrm{const}$ are concen-

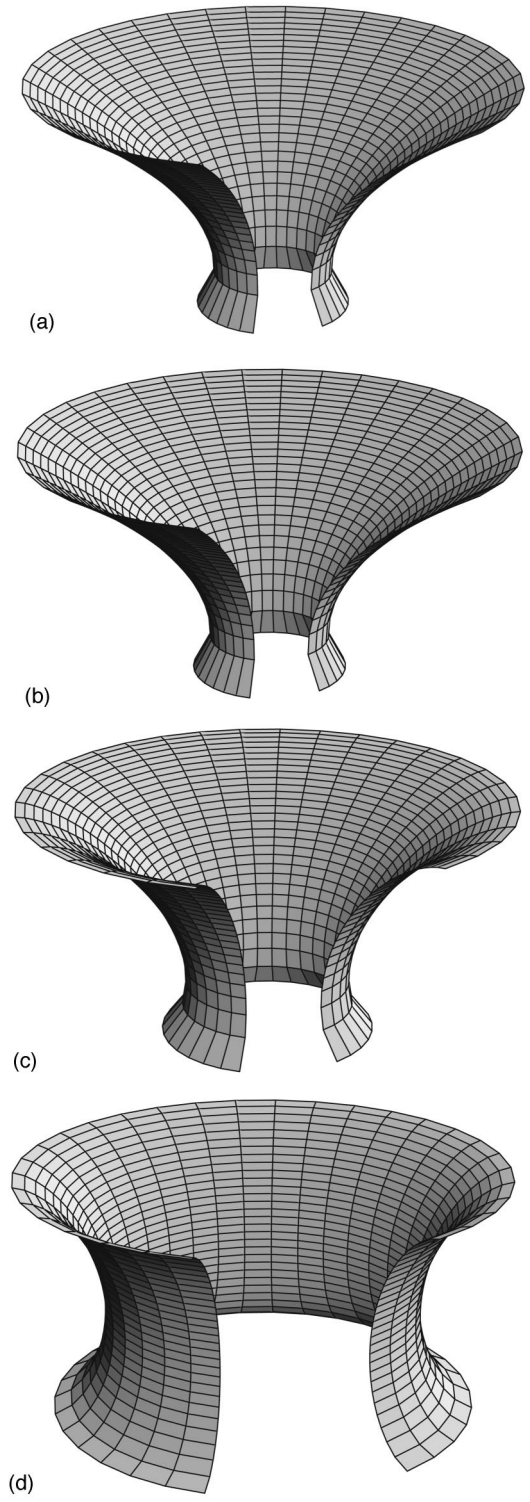

FIG. 11. Embedding diagrams of the optical reference geometry of the Schwarzschild–de Sitter spacetimes. The pure Schwarzschild case is taken for comparison in (a). The diagrams are given for (b) $y=10^{-6}$, (c) $y=0.002$, and (d) $y=0.03$. They are similar to the pure Schwarzschild case, because the region near the cosmological horizon being of highly different character is ''cut off'' by the limit of embeddability $y_{e(\mathrm{opt})}(r)$. Note that both ρ and z scales are adjusted so that all the plots occupy approximately the same area. For real proportions, see Fig. 13.

trated with an increasing density around $\rho=(-y)^{-1/2}$ as $r\to\infty$. Qualitative features of the modifications of the embedding diagrams of the optical geometry caused by $y\neq 0$ are illustrated by Fig. 13.

The optical geometry is well defined under the limit of embeddability again. Now, the ''tortoise'' coordinate is given by

$$r^*=D\left\{\ln|r-r_h|-\frac{1}{2}\ln\left(r^2+rr_h-\frac{2}{yr_h}\right)+\frac{6-r_h}{[(6+r_h)(2-r_h)]^{1/2}}\times\left\{\arctan\left[\left(\frac{2-r_h}{6+r_h}\right)^{1/2}\left(1+\frac{2r}{r_h}\right)\right]+E\right\}\right\}, \quad (62)$$

where

$$D=-\frac{2-r_h}{2yr_h(3+r_h)}, \quad E=-\sqrt{-y}[1+\ln(-4y)]. \quad (63)$$

We can see again that the black-hole horizon is infinitely far away at the optical geometry. Again, the optical space continues infinitely beyond the limit of embeddability as $r\to r_h$, and $r^*\to-\infty$, approaching asymptotically a geometry similar to Eq. (59).

V. LIMITS ON STATIC SPHERICALLY SYMMETRIC CONFIGURATIONS OF UNIFORM DENSITY

We shall focus our attention on an interesting connection between the limits of embeddability into the three-dimensional Euclidean space, and restrictions on the existence of static, spherically symmetric configurations of uniform density that are nonvacuum solutions of Einstein's equations with a nonzero cosmological constant. Our study is motivated by a conjecture of Kristiansson, Sonego, and Abramowicz [11] that the minimum radius of embeddability of the optical geometry coincides with the minimum radius of a static configuration of uniform density having the same spacetime parameters. This conjecture was verified for the Schwarzschild case [8,9], and the extreme Reissner-Nordström case [11,17]. Here, it will be tested in the case of the spherically symmetric spacetimes with a nonzero cosmological constant.

In the standard Schwarzschild coordinates, the line element of spherically symmetric static spacetimes can be given in the form

$$ds^2=-e^{2\Phi}dt^2+e^{2\Psi}dr^2+r^2(d\theta^2+\sin^2\theta\, d\phi^2), \quad (64)$$

where $\Phi=\Phi(r)$, $\Psi=\Psi(r)$. Solving the Einstein equations with $\Lambda\neq 0$ for a static configuration of constant density ϵ, the interior spacetime of the configuration of an outer radius R can be determined [18]. The radial metric coefficient is given by

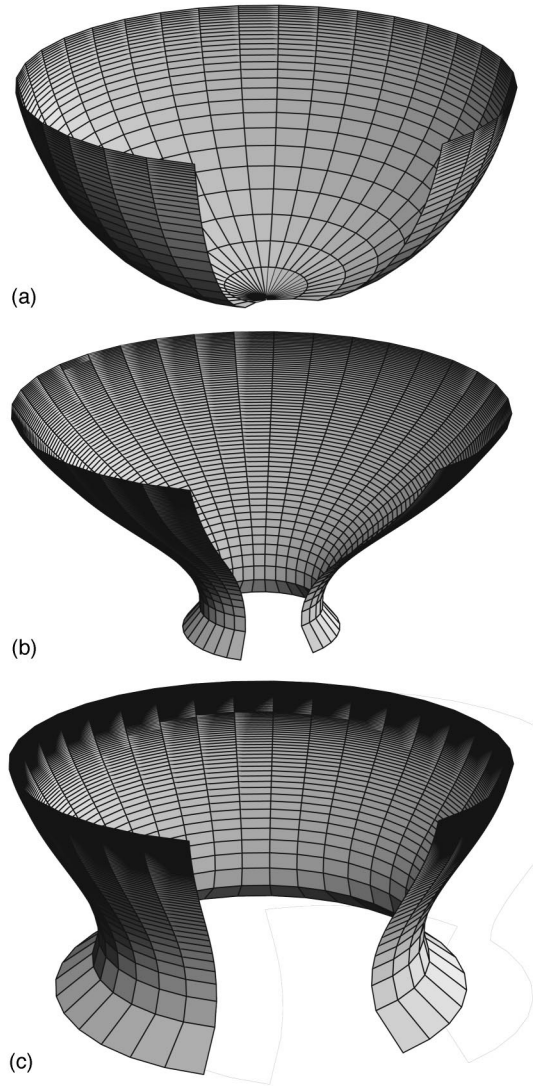

FIG. 12. Embedding diagrams of the optical geometry of the Schwarzschild–anti-de Sitter spacetimes. They are given for (a) $y=-10^{-6}$, (b) $y=-0.002$, and (c) $y=-0.03$. Contrary to the spacetimes with $y>0$, the diagrams cover whole asymptotic region of the optical geometry; however, it is stretched into finite region of the radial coordinate of the embedding Euclidean space. Note that both ρ and z scales are adjusted so that all the plots occupy approximately the same area. For real proportions, see Fig. 13.

$$e^{\Psi(r)}=\left(1-\frac{r^2}{\alpha^2}\right)^{-1/2}, \tag{65}$$

where $r<R$, and

$$\frac{1}{\alpha^2}=\frac{1}{3}(8\pi\epsilon+\Lambda). \tag{66}$$

Denoting

$$M=\frac{4\pi}{3}\epsilon R^3, \tag{67}$$

we find

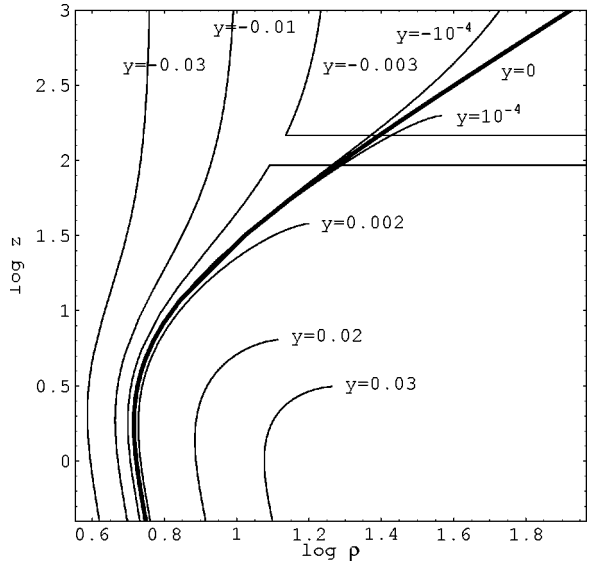

FIG. 13. Qualitative features of the embedding diagrams of the optical geometry of the Schwarzschild–de Sitter and Schwarzschild–anti-de Sitter spacetimes in a log-log diagram. The diagrams for $y\neq 0$ ''peel off'' the pure Schwarzschild diagram ($y=0$, bold curve). All sections with $y>0$ are complete (i.e., the maximum that can be embedded into Euclidean space is shown), except uninteresting lower parts of the diagrams. The diagrams are indicative for modifications of the spacetime structure caused by the presence of a cosmological constant.

$$e^{\Psi(R)}=\left(1-\frac{R^2}{\alpha^2}\right)^{-1/2}=\left(1-\frac{2M}{R}-\frac{1}{3}\Lambda R^2\right)^{-1/2}, \tag{68}$$

and we see immediately that the radial metric coefficient of the interior spacetime is smoothly matched to the corresponding metric coefficient of the exterior (vacuum) Schwarzschild–de Sitter or Schwarzschild–anti-de Sitter spacetime of the mass parameter M. The time component of the internal metric tensor is given by the relation

$$e^{\Phi(r)}=\frac{9M}{6M+\Lambda R^3}\left(1-\frac{2M}{R}-\frac{\Lambda}{3}R^2\right)^{1/2} -\frac{3M-\Lambda R^3}{6M+\Lambda R^3}\left(1-\frac{2Mr^2}{R^3}-\frac{\Lambda}{3}r^2\right)^{1/2}; \tag{69}$$

again, at $r=R$ we arrive at

$$e^{\Phi(R)}=\left(1-\frac{2M}{R}-\frac{\Lambda}{3}R^2\right)^{1/2}, \tag{70}$$

and the internal metric component is smoothly matched to the time metric coefficient of the external vacuum spacetime.

In the degenerated case, when the attractive cosmological constant and the parameters of the configuration are related by

$$\frac{1}{\alpha^2}=\frac{2M}{R^3}+\frac{\Lambda}{3}=0, \tag{71}$$

the internal spacetime is determined by the functions

$$e^{\Psi(r)}=1, \quad e^{\Phi(r)}=1+\frac{3M}{2R}\left(\frac{r^2}{R^2}-1\right); \tag{72}$$

notice that in this case the spacelike section $t=$const have purely three-dimensional Euclidean geometry. Of course, also these spacetimes are smoothly matched to the exterior Schwarzschild–anti-de Sitter spacetimes.

The limits on the allowed values of the outer radius of the static configurations follow from the reality conditions on the metric coefficients, i.e., $e^{\Psi(r)}\geqslant 0$ and $e^{\Phi(r)}\geqslant 0$ (see Ref. [18]). The results can be conveniently given in terms of the dimensionless cosmological parameter $y=\frac{1}{3}\Lambda M^2$ and dimensionless outer radius

$$x=\frac{R}{M}. \tag{73}$$

The condition $e^{\Psi(r)}\geqslant 0$ leads to a simple and natural restriction that the outer radius of the static configuration must be located in the static part of the external spacetimes. Therefore, the relevant restrictions are given by $e^{\Phi(r)}\geqslant 0$.

A. Repulsive cosmological constant ($y>0$)

Since $e^{\Phi(R)}>e^{\Phi(r)}>e^{\Phi(0)}>0$, the reality condition can be put into the form

$$[y-y_+(x)][y-y_-(x)]<0, \tag{74}$$

where

$$y_\pm(x)\equiv\frac{2x-9\pm 3|2x-3|}{2x^4} \tag{75}$$

and

$$y\leqslant y_s(x)\equiv\frac{1}{x^3}. \tag{76}$$

It follows from the relation (75) that

$$y_-(x)\equiv-\frac{2}{x^3}<y<y_+(x)\equiv\frac{4x-9}{x^4}. \tag{77}$$

For $y>0$ only $y_+(x)$ is relevant. Clearly, the function $y_+(x)$ corresponds just to the function $y_{e(\mathrm{opt})}(r)$ giving the limit of embeddability of the optical geometry. However, $y_+(x)$ is relevant only up to its maximum at $x_{\max}=3$, where $y_{\max}=1/27$. At $x\geqslant x_{\max}=3$, the function $y_s(x)$ is relevant. In this case, the outer radius of the static configuration is located just at the static radius r_s of the corresponding external Schwarzschild–de Sitter spacetime. The gravitational attraction acting on a test particle on the surface of the configuration is just compensated by the cosmological repulsion. (For $x>x_s$ the repulsion prevails, and a static configuration is possible only with a surface stress acting inwards. We shall not consider such a situation.) Therefore, for $0<y<1/27$, static configurations can exist, and their outer radius is limited both from below and from above. Only the lower limit coincides with the limit of embeddability of the optical geometry of the Schwarzschild–de Sitter spacetimes. The upper limit is different (see Fig. 1).

B. Attractive cosmological constant ($y<0$)

It is useful to introduce a family of critical values of the parameter y by the relation (given by $1/\alpha^2=0$)

$$y_{e(\mathrm{ord})}(x)\equiv-\frac{2}{x^3}. \tag{78}$$

Notice that the function $y_{e(\mathrm{ord})}(x)$ is not related to embeddability of the optical geometry, but, quite surprisingly, to embeddability function of the ordinary geometry $y_{e(\mathrm{ord})}(r)$, given by Eq. (44).

If $y>y_{e(\mathrm{ord})}(x)$, the relations (74) and (75) are valid; at $x\geqslant\frac{3}{2}$, $y_-(x)=y_{e(\mathrm{ord})}(x)$, while at $x\leqslant\frac{3}{2}$, $y_+(x)=y_{e(\mathrm{ord})}(x)$. For $x=\frac{3}{2}$, $y_-(x)=y_+(x)=-\frac{16}{27}$.

If $y<y_{e(\mathrm{ord})}(x)$, the relation (74) has to be replaced by the relation

$$[y-y_+(x)][y-y_-(x)]>0. \tag{79}$$

At $x>\frac{3}{2}$, $y_-(x)=y_{e(\mathrm{ord})}(x)$, $y_+(x)=(4x-9)/x^4$, while at $x<\frac{3}{2}$, $y_+(x)=y_{e(\mathrm{ord})}(x)$ and $y_-(x)=(4x-9)/x^4$. By putting all the conditions together (see Ref. [18] for details) we arrive at a relatively simple conclusion that for both $y>y_{e(\mathrm{ord})}(x)$ and $y<y_{e(\mathrm{ord})}(x)$ the limit on the outer radius of the static configurations is given by

$$y<\frac{4x-9}{x^4}. \tag{80}$$

Now, it is related to the limit of embeddability of the optical geometry of the Schwarzschild–anti-de Sitter spacetimes (see Fig. 4).

In the special class of the static configurations with their constant density ϵ related to the attractive cosmological constant by

$$\Lambda_{e(\mathrm{ord})}=-8\pi\epsilon, \tag{81}$$

the outer radii of these configurations are determined by the condition

$$y=y_{e(\mathrm{ord})}(x)=-\frac{2}{x^3}. \tag{82}$$

In this degenerated case, the metric coefficients are given by Eq. (72). The restriction $e^{\Phi(0)}>0$ then implies

$$x>\frac{3}{2}. \tag{83}$$

Clearly the special class of static configurations with $y=y_{e(\mathrm{ord})}(x)$, corresponding to the limit of embeddability of the ordinary geometry induced on the $t=$const sections of the Schwarzschild–anti-de Sitter spacetimes, are allowed at $R>3M/2$ only, and for the cosmological parameter satisfying the conditions

$$-\frac{16}{27}<y<0. \tag{84}$$

VI. CONCLUDING REMARKS

Both a repulsive or an attractive cosmological constant lead to significant changes of the structure of the Schwarzschild spacetimes containing black holes. In fact, for any repulsive cosmological constant $y>y_{\rm crit}=1/27$, the spacetime contains no black-hole horizon, and the metric (1) governs a naked singularity in a dynamic universe. For $0<y<y_{\rm crit}$, the spacetime is dynamic under the black-hole horizon, and above the cosmological horizon. For $y<0$, a black-hole horizon always exists; the spacetime is static everywhere above the horizon, but its asymptotic structure differs significantly from the limiting Schwarzschild case.

It has been shown that the influence of a nonzero cosmological constant reflects itself in properties of the motion of test particles and photons, the photon escape cones, and the embedding diagrams. Surprisingly, all the properties keep the same character as in the Schwarzschild case at $r=3M$ and its vicinity; the photon circular orbits exists there independently of values Λ and M, if $y<y_{\rm crit}$. Moreover, at $r=3$, the turning point of the throat of embedding diagrams of the optical geometry exists for all values of y, and the centrifugal force related to the optical geometry reverses its sign there.

The differences appear and grow with distance growing from $r=3M$. It is intuitively clear that the regions of the Schwarzschild–de Sitter and Schwarzschild–anti-de Sitter spacetimes similar to the corresponding regions of the Schwarzschild spacetime can exist for the parameter y small enough. Such regions can be easily estimated for the Schwarzschild–de Sitter spacetimes. We can consider them similar to the Schwarzschild spacetime in some regions, if they allow existence of stable circular orbits, i.e., if their parameter $y<y_{c({\rm ms})}=12/15^4$.

The effective potential of the test-particle motion (see Fig. 2) gives an indication that the structure of the Schwarzschild–de Sitter spacetime is significantly different from the structure of the pure Schwarzschild spacetime above the static radius, i.e., at $r>r_s=y^{-1/3}$. Notice that for $y\ll 1$, the outer boundary of stable circular orbits can be estimated as $r_{\rm ms(out)}\sim(4y)^{-1/3}\sim r_s/4^{1/3}$. These estimates can be, moreover, supported by the character of the embedding diagrams.

First, one can see (Fig. 11) that strong differences in the behavior of the embedding diagrams of the ordinary geometry of the Schwarzschild–de Sitter and Schwarzschild spacetimes occur at $r>r_s$. This is confirmed by the behavior of the embedding diagrams of the optical reference geometry (Fig. 12); we even obtain an exact criterion—namely, the limit of embeddability given by Eq. (54). For $y\ll 1$, the outer limit of embeddability can be estimated as $r_{\rm em(out)}\sim(4/y)^{1/3}\sim 4^{1/3}r_s$. Therefore, we can propose a criterion for the boundary of the region of strong deviations between the structure of the Schwarzschild–de Sitter and Schwarzschild spacetimes to be the outer limit of embeddability of the optical geometry. In the case of the Schwarzschild–anti-de Sitter spacetimes one can propose an analogous criterion for the region of strong deviations from the pure Schwarzschild spacetime, namely, the outer limit of embeddability of the ordinary geometry $r_{e({\rm ord})}=(-2/y)^{1/3}$.

Note that the inner limit of embeddability of the optical geometry of both the Schwarzschild–de Sitter and Schwarzschild–anti-de Sitter spacetimes coincide with the inner limit on the existence of the static, spherically symmetric configurations of uniform density; this fact is in agreement with the conjecture of Kristiansson, Sonego and Abramowicz [11]. However, in the Schwarzschild–de Sitter spacetimes this coincidence does not hold in the case of the outer limit. The outer limit of embeddability of the optical geometry can be comparable with the outer radius of the static configurations only in situations where an inward-directed surface tension of the static configuration compensates the influence of the cosmological repulsion.

ACKNOWLEDGMENTS

The present work has been supported by the Czech Republic Grants No. J 10/98:192400004 and GACR 202/99/0261. The authors would like to express their gratitude to Professor Marek A. Abramowicz for stimulating discussions.

[1] L. M. Krauss and M. S. Turner, Gen. Relativ. Gravit. **27**, 1137 (1995).
[2] J. P. Ostriker and P. J. Steinhart, Nature (London) **377**, 1137 (1995).
[3] L. M. Krauss, Astrophys. J. **501**, 461 (1998).
[4] A. Sen, ''Developments in Superstring Theory,'' hep-ph/9810356v2, 1998.
[5] Z. Stuchlík, Bull. Astron. Inst. Czech. **35**, 205 (1984).
[6] Z. Stuchlík, Bull. Astron. Inst. Czech. **34**, 129 (1983).
[7] J. B. Zel'dovich and I. D. Novikov, *Stroenie i Evolyutsia Vselennoy* (Nauka, Moscow, 1975).
[8] C. W. Misner, K. S. Thorne, and J. A. Wheeler, *Gravitation* (Freeman, San Francisco, 1973).
[9] M. A. Abramowicz, B. Carter, and J. P. Lasota, Gen. Relativ. Gravit. **20**, 1173 (1988).
[10] Z. Stuchlík and S. Hledík, ''Embedding diagrams of the optical geometry in Kerr backgrounds,'' Report No. TPA 009, Silesian University at Opava, 1998.
[11] S. Kristiansson, S. Sonego, and M. A. Abramowicz, Gen. Relativ. Gravit. **30**, 275 (1998).
[12] M. A. Abramowicz and A. R. Prasanna, Mon. Not. R. Astron. Soc. **245**, 720 (1990).
[13] M. A. Abramowicz, J. C. Miller, and Z. Stuchlík, Phys. Rev. D **47**, 1440 (1993).
[14] M. A. Abramowicz, Mon. Not. R. Astron. Soc. **245**, 733 (1990).

[15] M. A. Abramowicz, Mon. Not. R. Astron. Soc. **256**, 710 (1992).
[16] Z. Stuchlík, Bull. Astron. Inst. Czech. **41**, 341 (1990).
[17] F. De Felice, Y. Yu, and J. Fang, Mon. Not. R. Astron. Soc. **277**, 217 (1995).
[18] Z. Stuchlík, ''Spherically symmetric static configurations of uniform density in spacetimes with a non-zero cosmological constant,'' Report No. TPA 007, Silesian University at Opava, 1998.